Physica Scripta

PAPER

Tuning of band gap by anion variation of Ga_2TiX_6 (X = Cl, Br, I) for solar cells and renewable energy

RECEIVED
18 April 2022

REVISED
14 June 2022

ACCEPTED FOR PUBLICATION
6 July 2022

PUBLISHED
18 July 2022

Tahani I Al-Muhimeed[1], Jameelah Alzahrani[2], Syed Awais Rouf[3,*], Samah Al-Qaisi[4], Radhakrishnan Anbarasan[5], Q Mahmood[2], Hind Albalawi[6], Sarah Alharthi[7], Mohammed A Amin[7], H H Somaily[8,9] and Manal Morsi[10,11]

[1] Department of Chemistry, College of Science, King Saud University, PO Box 22452, Riyadh 11495, Saudi Arabia
[2] Basic & Applied Scientific Research Center, and Department of Physics, College of Science, Imam Abdulrahman Bin Faisal University, PO Box 1982, 31441 Dammam Saudi Arabia
[3] Department of Physics, Division of Science and Technology, University of Education, Lahore, Pakistan
[4] Palestinian Ministry of Education and Higher Education, Nablus, Palestine
[5] SSN Research Centre, Sri Sivasubramaniya Nadar College of Engineering, Chennai, Tamilnadu, 603 110, India
[6] Department of Physics, College of Sciences, Princess Nourah bint Abdulrahman University (PNU), PO Box 84428, Riyadh, 11671, Saudi Arabia
[7] Department of Chemistry, College of Science, Taif University, PO Box 11099, Taif 21944, Saudi Arabia
[8] Research Center for Advanced Materials Science (RCAMS), King Khalid University, Abha 61413, PO Box 9004, Saudi Arabia
[9] Department of Physics, Faculty of Science, King Khalid University, PO Box 9004, Abha, Saudi Arabia
[10] Department of Physics, College of Arts and Science, Wadi Addawasir, Prince Sattam bin Abdulaziz University, Saudi Arabia
[11] Department of Physics, Girl College for Art, Science, and Education, Ain-Shams University, Cairo, Egypt
[*] Authors to whom any correspondence should be addressed.

E-mail: syedawais.rouf@ue.edu.pk

Keywords: density functional theory, solar cells, thermoelectric, renewable energy, figure of merit

Abstract

Vacancy-ordered double perovskites have been studied vastly for energy applications for the last few decades. In this article, we have investigated the optical and thermoelectric characteristics of Ga_2TiX_6 (X = Cl, Br, I). The phonons dispersions, formation energy, and tolerance factors reveal dynamic and structural stabilities. The predicted band gaps turn out to be 2.74 eV, 2.0 eV, and 1.32 eV for Ga_2TiCl_6, Ga_2TiBr_6, and Ga_2TiI_6, respectively, corresponding to the absorption bands 275 nm to 413 nm, 365 nm to 539 nm, and 413 nm to 689 nm. Therefore, the absorption band in the entire visible region for Ga_2TiI_6 makes it an excellent material for solar cells. The optical characteristics are explained by dielectric constants (ε_1, ε_2), absorption coefficient, and dielectric constants. Thermoelectric efficiency is addressed by calculating the figure of merit to highlight the potential of the investigated materials for thermoelectric applications.

1. Introduction

Recently, solar energy has become the focus of attention of the scientific community because of the shortage of energy sources and increasing consumption. Solar energy is a clean, renewable energy source that eliminates traditional energy sources like fossil fuels, coal, natural gas, etc [1–3]. Thermoelectric energy is also a promising renewable energy source that converts heat directly into valuable electrical energy. Therefore, to meet these challenges, various materials have been explored for solar cells and thermoelectric generators [4].

The perovskite halides having the formula ABX_3, where A = CH_3NH_3, Pb^{2+}, Sn^{2+}, and X = halogen atoms, can be categorized into two main types organic based and inorganic-based perovskites [5]. The double perovskites combine two single perovskites, which are more stable and reliable for technological applications. The usual formula for single perovskite is ABX_3, and double perovskites is $A_2B'B''X_6$. In this formula the octahedral cations B′ and B″ are different elements, and 6-fold coordinates of X atoms surround each one. On the other hand, for the same octahedral cations, each atom is divided by 12-fold coordinates of X atoms and then taken as the average. This new type of perovskites, A_2BX_6 is studied as vacancy-ordered double perovskites [6].

The perovskite halides $CH_3NH_3PbX_3$ (X = Br, I) had been used in place of dye-sensitized solar cells up to 2009, but due to lower efficiency of ~3.8% and stability, they could not gain extensive consideration [7]. The perovskites solar cells (PSCs) are trying to develop by substituting a liquid electrolyte with a solid hole transport layer up to 2012, which directly increased the efficiency. This efficiency improvement increased perovskite to some extent [8–10]. Recently, PSCs efficiency has been improved to 25.5%, which is greater than the silicon-based conventional solar cells [11]. The lifetime of PSCs is nearly 1 year, while the silicon solar cell has a working capacity of 25 years. The environmental factors like temperature, intense light, moisture, and oxygen decompose the organic part. The most terrible factor is moisture that hydrates the solar cells to damage their crystal structures [12]. For the improvement of stability, the following techniques are constructing new stable halide perovskite [13, 14], applying charge transport layers of stable inorganic materials [15], the development of crystals structure by doping [16]. The above techniques can increase the lifetime up to a limited period. For long-term stability, we must adopt advanced procedures.

The toxic nature of lead is also a major restriction in the commercialization of PSCs. The lead contents spread pollution in the atmosphere, creating clouded consciousness, fatigue, clumsiness, and muscle weakness [17]. Many attempts have been made to construct low-toxic or non-toxic halide perovskites for solar cells industry [18–20]. An effort has also been made to replace Pb^{2+} ions with other Sn^{2+} and Ge^{2+} ions of the same group. The Sn^{2+} and Ge^{2+} have the legacy of oxidizing 5 s orbitals to destabilize the materials of the solar cell in the ambient atmosphere [19, 20]. Therefore, the doping procedure could not resolve the issues of toxicity and stability.

In the last decade, double perovskites $A_2B(I)B'(III)X_6$ and their vacancy-ordered derivatives $A_2B(IV)X_6$ are anticipated stable alternatives of organic-inorganic and lead-containing perovskites. In these materials, toxic lead ions are replaced by the monovalent, trivalent, and tetravalent ions along with ordered vacancy to maintain the charge balance. The double perovskites have exceptional stability, environment friendly and tunable characteristics. A number of researchers have explored double perovskites like Rb_2PdBr_6 and Cs_2PtI_6 investigated for solar cells because of their optimum band gaps of 1.3 eV and 1.22 eV, respectively [21]. The maximum absorption band and ultralow values of lattice thermal conductivity increase their use for renewable energy.

The double perovskites existing vacancy at octahedral cations (B) positions are considered exceptional materials for optoelectronics. Zhou *et al* proposed using $Cs_2SnCl_{6-x}Br_x$ for photodetectors in the cubic phase after a successful experiment [22, 23]. The Cs_2SnI_6 having band gap E_g = ~1.2 eV is promising for optoelectronics. Moreover, the stable crystal structure, non-toxic nature, covalent bonding, and band gap in the visible region enhance efforts for its commercialization [24–26]. The lead-free double perovskites approach to efficiency of 11.2%, which is significantly less than Pb-based PSCs [27]. Zhao *et al* theoretically explored the In_2TiX_6 (X = Cl, Br, I) [28]. However, researchers have performed much work to improve the efficiency of lead-free perovskites [29]. The experimental and theoretical literature on Ga_2TiX_6 (X = Cl, Br, I) is not found. However, we have explored these compounds theoretically based on their family of compounds which have rich literature. Our findings will provide the opportunity to the researchers to realize them for solar cells and thermoelectric applications.

2. Method of calculation

The structural optimization, electronic, and optical properties of Ga_2TiX_6 (X = Cl, Br, I) are computed by Wien2k code [30]. Perdew–Burke–Ernzerhof Generalized-Gradient Approximation, PBE-GGA analyzes the structural properties because it accurately computes the structural parameters but underestimates the electronic band gap. The mBJ potential is most versatile, easy to execute, and has a lower computational cost, which accurately computes the band gaps of the semiconductors and insulators. Its accuracy is equivalent to HSE06; therefore, we prefer the calculations with mBJ potential. Therefore, to precisely obtain the electronic band gap, we have applied Becke and Johnson potential given by Trans and Blaha, TB-mBJ [31]. This potential average the interatomic distance among atoms and accurate the band gap. However, HSE06 and GGA + U approaches are also suitable for band gap accuracy, but HSE06 has more computational cost than TB-mBJ, and GGA + U is implemented in heavy transition metals. The TB-mBJ has low computational cost, is friendly, and has similar accuracy as HSE06 [32]. Moreover, to incorporate spin–orbit coupling (SOC), we have run the calculations with TB-mBJ + SOC, which has a minute difference from TB-mBJ potential calculations. The $R_{MT}xK_{max}$, l_{max}, G_{max} (10, 8, 16) are incorporated in input files, where R_{MT} muffin-tin radius, K_{max} maximum wave vector, l_{max} angular momentum, and G_{max} gaussian factor. The convergence of energy has been executed as 0.00001 Ry, and Monkhorst-Pack order 20 × 20 × 20 is taken for convergence of charge to compute optical properties and 30 × 30 × 30 for thermoelectric properties. Thermoelectric properties are executed by BoltzTraP code which

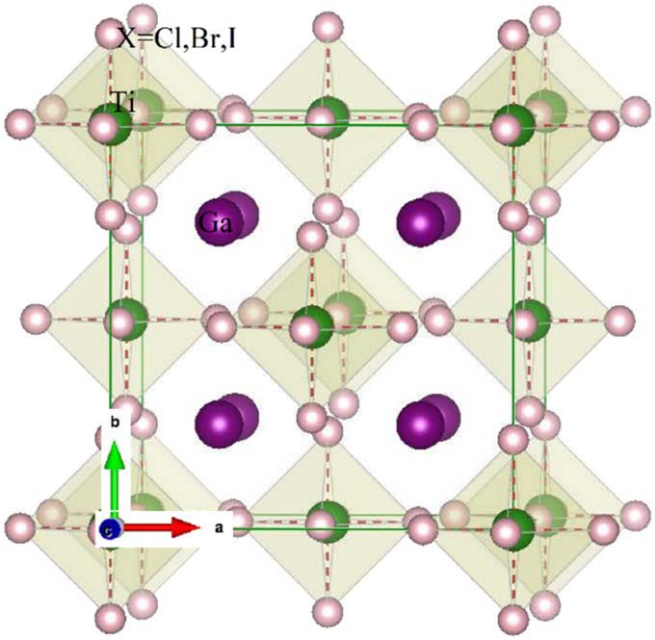

Figure 1. Crystal structure of Ga_2TiX_6 (X = Cl, Br, I) developed by VESTA Software.

Table 1. The calculated parameters of Ga_2TiCl_6, Ga_2TiBr_6, and Ga_2TiI_6.

Parameters	Ga_2TiCl_6	Ga_2TiBr_6	Ga_2TiI_6
lattice constant a_o (Å)	10.39	11.07	12.08
bulk modulus B_o (GPa)	33.47	24.61	17.68
Formation energy H_f (eV)	−3.0	−2.78	−2.58
Band gap E_g (eV)	2.74	2.00	1.32
Static dielectric constant ε_1 (0)	3.93	3.98	5.29
Static refractive index n (0)	1.98	2.00	2.30
Reflectivity R (0)	0.108	0.110	0.155
Effective mass of electrons (m_e^*)	$0.39m_0$	$0.34m_0$	$0.21m_0$
Effective mass of holes (m_h^*)	$1.2\ m_0$	$0.8\ m_0$	$0.45\ m_0$

analyzes them based on Boltzmann transport theory. The relaxation has been kept constant during computations as $\tau = 10^{-14}$s [33].

3. Results and discussion

3.1. Structural and electronic properties

The cubic crystal structures of Ga_2TiX_6 (X = Cl, Br, I) in polyhedral form with space group $Fm\bar{3}m$, (No.225) are shown in figure 1. The cubic crystal structures are taken from the materials project [34]. The 12-fold coordinates of X atoms separate the octahedral Ti atoms from each other, and Ga atoms fill the space between them. The 12 and 6 X atoms surrounded Ga, and Ti, respectively. The started Wyckoff positions for Ga 8c (1/4, 1/4, 1/4), Ti (0, 0, 0), and X 24e (0.21, 0, 0). The computed lattice constants (a_o) from optimized structures are shown in table 1, which increase from Cl to I because of increasing additional shells. The bulk moduli (B_o) trends are opposite to lattice constants (a_o), decreasing from Cl to I. Ga is found primarily in +3 oxidation state, but its +1-oxidation state is also frequently studied, e. g a very stable compound $GaCl_2$ contains both gallium(I) and gallium (III) and is formulated as $GaIGaIIICl_4$ [35]. In our double perovskites number of studies are verified experimentally, such as Cs_2SnBr_6 nanocrystals [36].

Before addressing the applications of these compounds, the confirmation of stability is essential. The tolerance factor t_F is computed by atomic radius calculations through the relation,

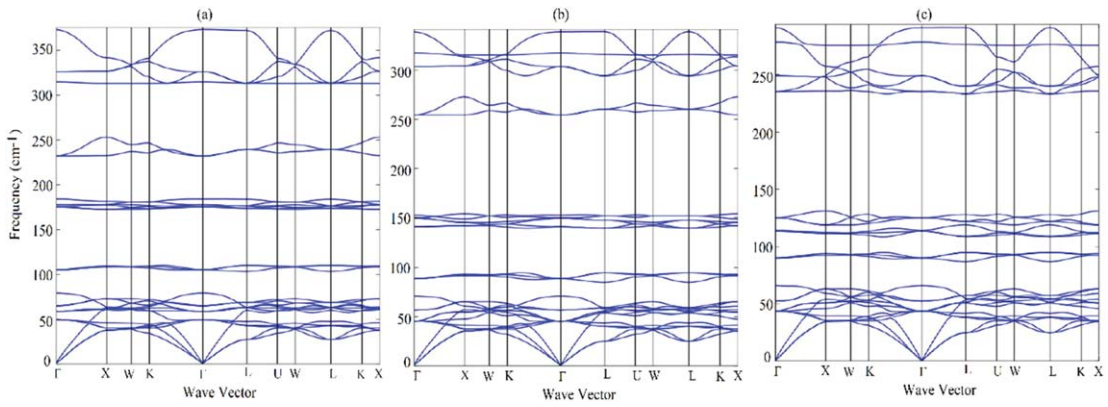

Figure 2. Phonon band structures of (a) Ga_2TiCl_6, (b) Ga_2TiBr_6, and (c) Ga_2TiI_6.

$$t = (r_{Ga} + r_X)/\sqrt{2}\,(r_{Ti} + r_X) \tag{1}$$

where r_{Ga}, r_{Ti} and r_X show atomic radii of Ga, Ti, and X [37]. The findings of t_F are shown in table 1 which are extremely near to ideal values (unity). Therefore, the structures of studied materials are stable. We have computed the energies of compounds $GaTi_2Cl_6$, $GaTi_2Br_6$, $GaTi_2I_6$ and individual elements Ga, Ti, Cl/Br/I through the optimization process. Then the formation energy has been evaluated from the relations

$$\Delta H_f = E_{Total}(Ga_l Ti_m X_n) - lE_{Ga} - mE_{Ti} - nE_X \tag{2}$$

Here $E_{Total}(Ga_l Ti_m X_n)$ represent the total energy of compounds $GaTi_2X_6$ (X = Cl, Br, I) while E_{Ga}, E_{Ti} and E_X represents the energies of Ga, Ti, and X atoms. The *l*, *m*, and *n* show the number of aa, Ti, and X, atoms, respectively. The computed values of ΔH_f are shown in table 1. The negative energies confirm the release of energy during compounds formation and thermally stabilize the structures [38–40]. Moreover, thermodynamic stability is also confirmed from the positive frequencies of the phonon's dispersion.

In materials the lattice vibration take place due to individual atoms kinetic energies. This lattice vibration generates elastic waves in the materials which overlap. If the frequencies of phonons are negative, their wave interaction is abrupt, destabilizing the structures, and if it is positive, then phonons waves cancel each other effect and stabilize the materials structures. The phonons band structures for Ga_2TiCl_6, Ga_2TiBr_6, and Ga_2TiI_6 are plotted in figures 2(a)–(c). The positive frequencies for all the band structures confirm the dynamic stability. The symmetry of structures generates total 27 phonons, from which 3 phonons are acoustic, and the remaining are optical. The low-frequency phonons meet at Γ direction and diminish each other [41, 42].

For the electronic properties discussion, band structures without SOC and with SOC are presented in figures 3(a)–(c). The band gap was reduced to 0.05 with SOC as compared to without SOC. Therefore, the effect of SOC on studied materials is minimal. The band gaps are reported at 2.74 eV, 2.0 eV, and 1.32 eV for Ga_2TiCl_6, Ga_2TiBr_6, and Ga_2TiI_6, respectively. The Ga_2TiCl_6 has an indirect band gap at Γ-X symmetry while Ga_2TiBr_6 and Ga_2TiI_6 have direct band gaps at Γ-Γ symmetry. Therefore, the band gap of 1.32 eV for Ga_2TiI_6 is ideal for solar cells. The effective masses of electrons and holes for Ga_2TiCl_6, Ga_2TiBr_6, and Ga_2TiI_6 are computed (see table 1). The low values of effective masses show that the studied double perovskites are promising for solar cells. The density of states for compounds and atoms (Ga, Ti, X) are plotted in figures 4(a)–(c). At the valence band, the DOS of halogen (X) atoms are present, while at the conduction band, the DOS of Ti atoms are present. The DOS of Ga also exists but in the deep levels of conduction bands. Therefore, the transitions of electrons are possible from X atoms to Ti due to the p-d hybridization of p-states of X atoms and d states of Ti atoms. The states at valence band maxima cross a bit because of density functional theory-based approximations and their p-type character. In p-type semiconductors, some shallow level states appear just above the valence band from which carriers can make transitions.

3.2. Optical properties

The optical properties of Ga_2TiX_6 (X = Cl, Br, I) are analyzed by dielectric constants and their dependent parameters, which are computed from the relations taken from [43–46]. The computed plots of optical characteristics are presented in figures 5(a)–(d) and figures 6(a), (b). The band gaps of Ga_2TiCl_6, Ga_2TiBr_6, and Ga_2TiI_6 are 2.74 eV, 2.0 eV, and 1.32 eV, respectively. The band gap of 1.32 eV of Ga_2TiI_6 is ideal for solar cell applications [47]. Therefore, light's dispersion, absorption, and reflection are addressed systematically. The real dielectric constant $\varepsilon_1(\omega)$ regulates light distribution at the resonance frequency. The maximum scattering of light has been observed at resonance energies 3.2 eV (6.4), 2.5 eV (6.9), and 1.8 eV (8.0) for Ga_2TiCl_6, Ga_2TiBr_6,

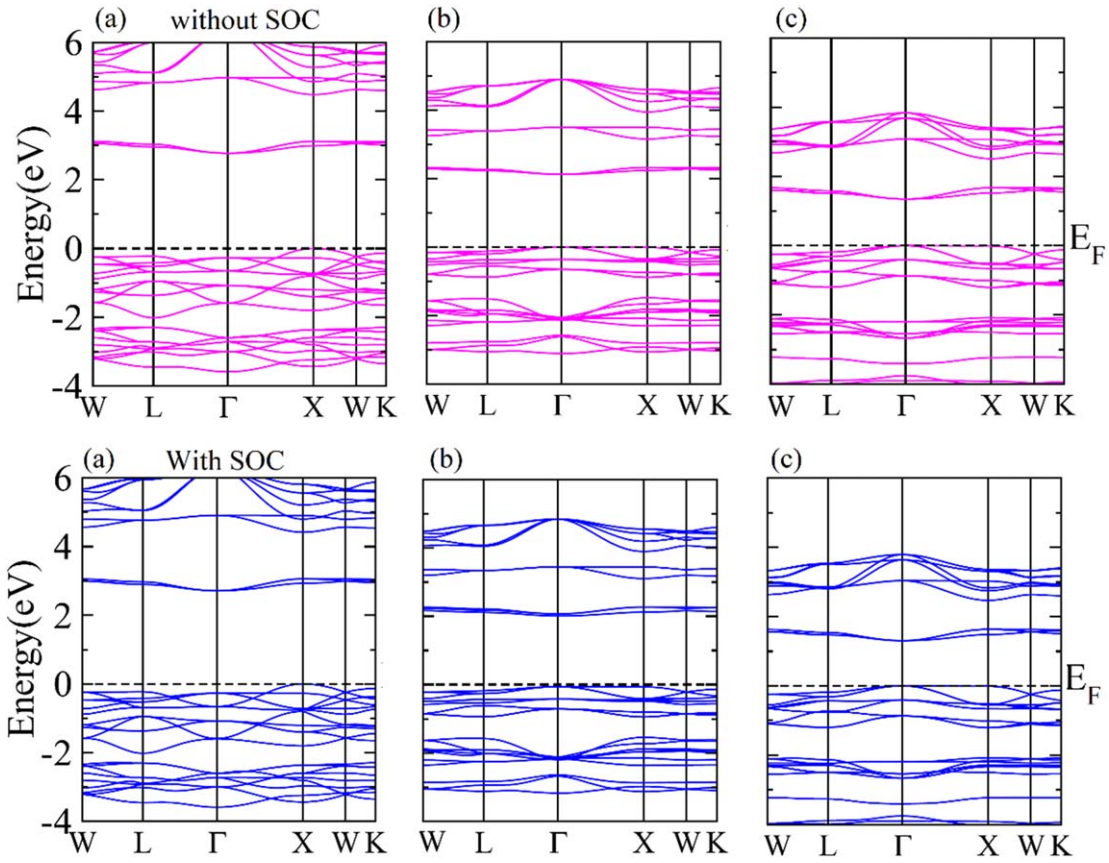

Figure 3. The band structures of (a) Ga_2TiCl_6, (b) Ga_2TiBr_6, and (c) Ga_2TiI_6 [without SOC (pink color), and with SOC (blue color)].

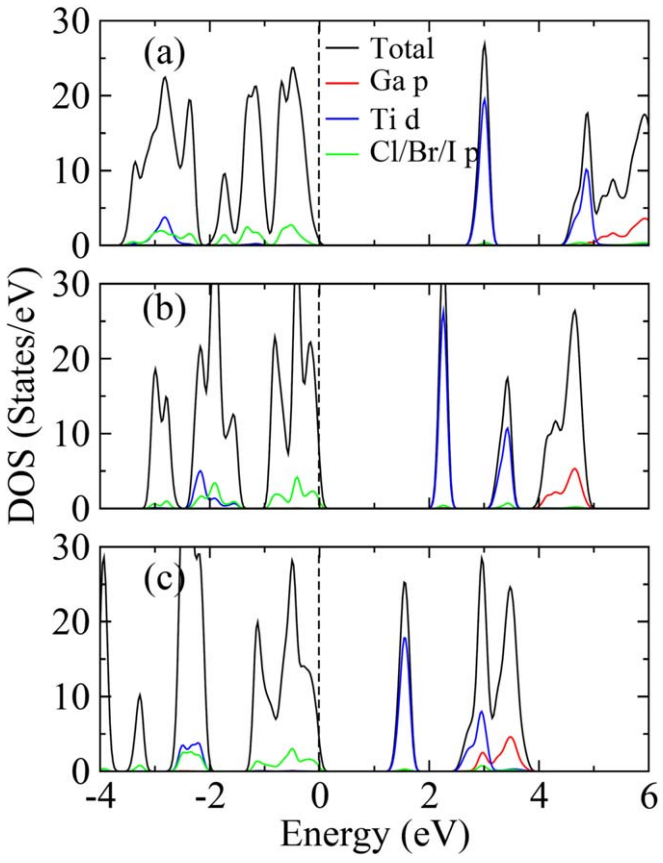

Figure 4. The density of states of (a) Ga_2TiCl_6, (b) Ga_2TiBr_6, and (c) Ga_2TiI_6.

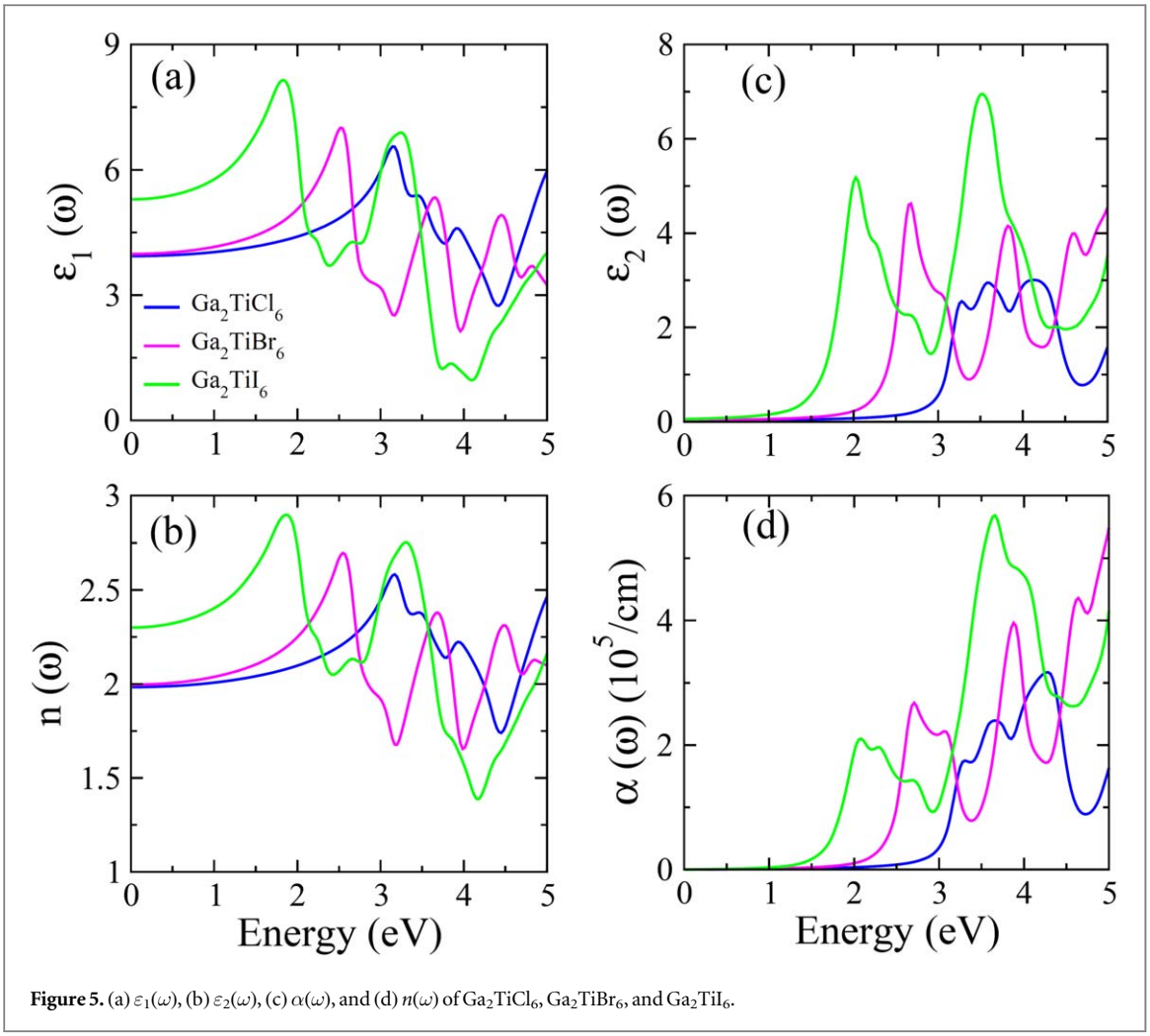

Figure 5. (a) $\varepsilon_1(\omega)$, (b) $\varepsilon_2(\omega)$, (c) $\alpha(\omega)$, and (d) $n(\omega)$ of Ga_2TiCl_6, Ga_2TiBr_6, and Ga_2TiI_6.

and Ga_2TiI_6 as described in figure 5(a). The peaks of the minimum intensity of $\varepsilon_1(\omega)$ have been found at 4.4 eV (2.7), 3.2 eV (2.5), and 2.4 eV (3.6) for Ga_2TiCl_6, Ga_2TiBr_6, and Ga_2TiI_6, respectively. The $\varepsilon_1(0)$ rises from 3.93 to 5.29 by the substitution of Cl with Br/I, which is inversely connected with the optical band gap and satisfies the Penn's model [48],

$$\varepsilon_1(0) \approx 1 + \left(\frac{\hbar\omega_p}{E_g}\right)^2 \tag{3}$$

Where $\varepsilon_1(0)$ is the value of real dielectric constant at zero frequency, $\hbar\omega_p$ is the energy of phonons, E_g is the band gap. At fixed energy the relation, the $\varepsilon_1(0)$ and E_g according to Penn's relations. From Cl to I, Eg decreases and value of $\varepsilon_1(0)$ increases (See table 1).

The refractive index n(ω) is also evaluating the dispersion of light and replica of $\varepsilon_1(\omega)$ (See figure 5(b)). Therefore, n (0) and $\varepsilon_1(0)$ are according to formula $n_0^2 = \varepsilon_1(0)$. The value of n(ω) is higher for Ga_2TiI_6 as compared to Ga_2TiCl_6 and Ga_2TiBr_6 which shows that the increasing size of halide ions increases the dispersion (See table 1). The imaginary dielectric constant $\varepsilon_2(\omega)$ has been extracted from $\varepsilon_1(\omega)$ by Krammer-Kronge relation [49].

It calculates the dilution of light when it passes through the material whose threshold limits on energy axis 2.74 eV, 2.0 eV and 1.32 eV are well consistent with band gap of materials. The computed values are shown in figure 5(c) in which the first absorption band bands are Ga_2TiCl_6 (3.1 eV to 4.7 eV), Ga_2TiBr_6 (2.3 eV to 3.7 eV) and Ga_2TiI_6 (1.6 eV to 3.0 eV). Therefore, the Ga_2TiCl_6, Ga_2TiBr_6, and Ga_2TiI_6 absorb light in the ultraviolet, near visible, and visible regions.

The absorption coefficient $\alpha(\omega)$ calculates the absorption of photons energy by electrons. Its values are computed by dielectric constants through equation [50],

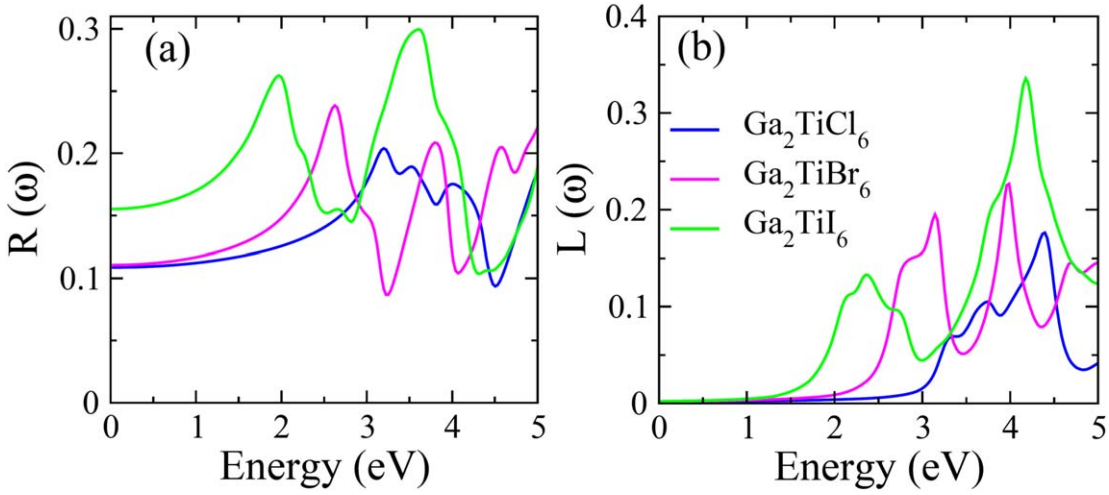

Figure 6. (a) Reflectivity R (ω) and (b) optical loss factor L (ω) of Ga_2TiCl_6, Ga_2TiBr_6, and Ga_2TiI_6.

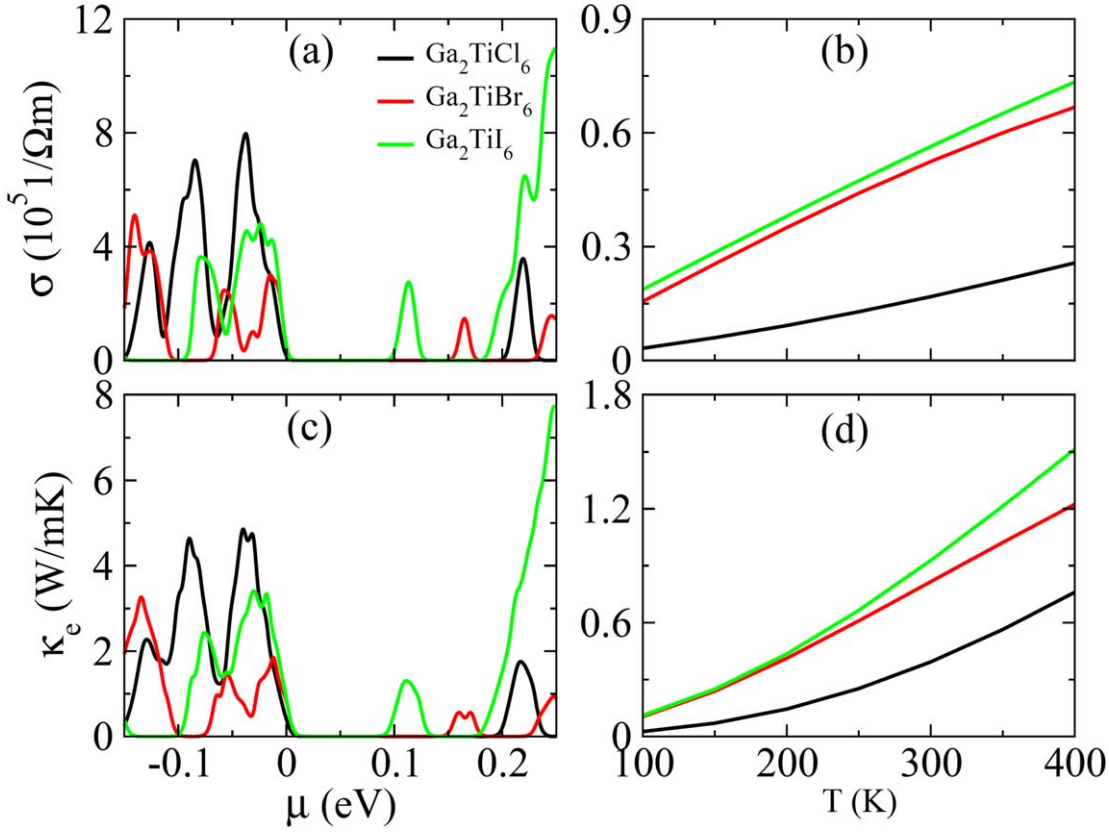

Figure 7. (a), (b) Electrical conductivity (σ) and (c), (d) Thermal conductivity (κ) of Ga_2TiCl_6, Ga_2TiBr_6, and Ga_2TiI_6 are computed versus μ (eV) and T (k).

$$\alpha(\omega)_i = \frac{2\omega}{c}\left(\frac{-Re(\varepsilon(\omega)_i) + |\varepsilon(\omega)_i|}{2}\right)^{\frac{1}{2}} \tag{4}$$

The absorption peaks of maximum intensity are found in the ultraviolet range (See figure 5(d)) for Ga_2TiCl_6 and Ga_2TiBr_6 and in the visible range for Ga_2TiI_6.

The light interacts with the materials surface and the surface behavior is measured in terms of reflectivity. The computed values of R (ω) are presented in figure 6(a) and its R (0) values are depicted as 0.108, 0.110 and 0.155 for Ga_2TiCl_6, Ga_2TiBr_6, and Ga_2TiI_6, respectively. The behavior of R (ω) is linked with a real dielectric constant showing maximum reflectivity values where dispersion is maximum. During the contact of light with

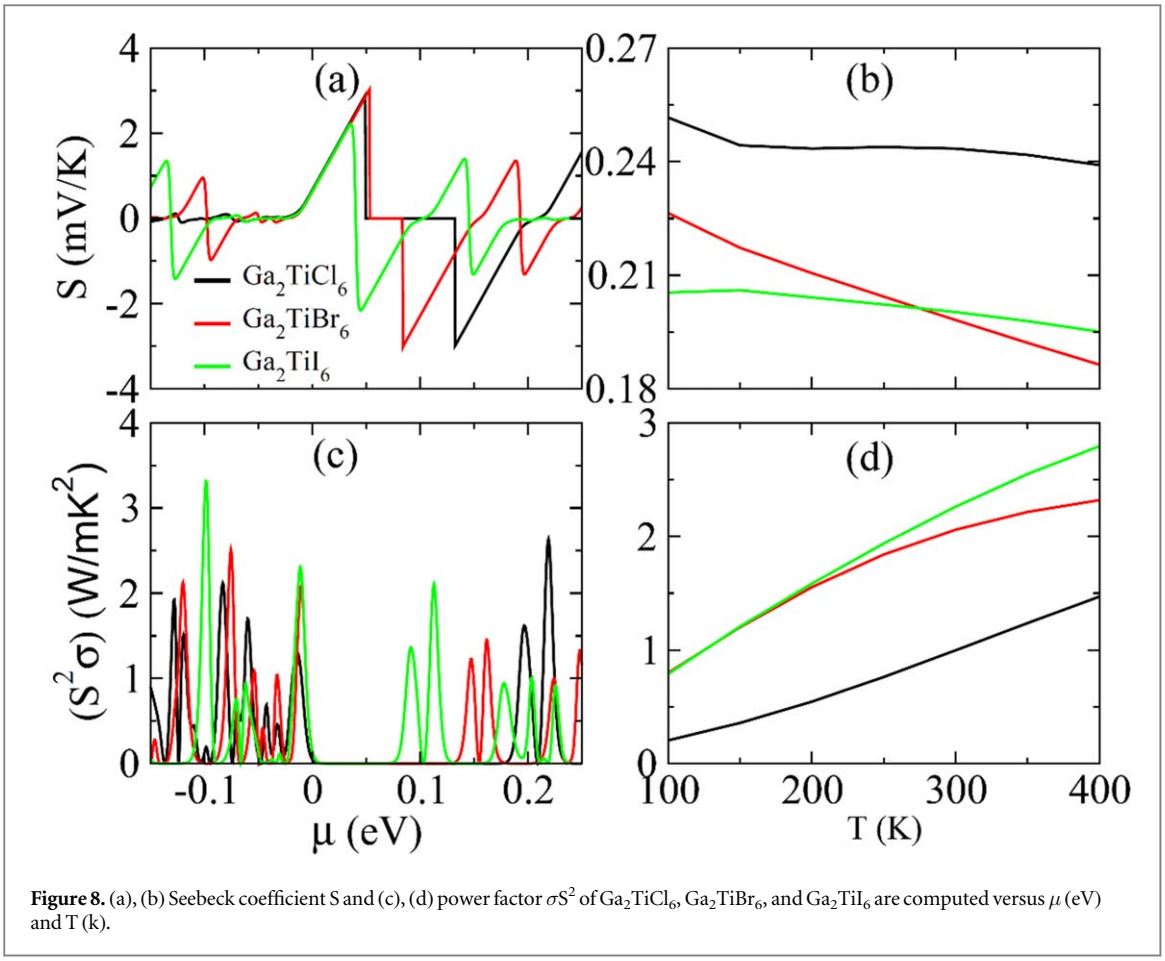

Figure 8. (a), (b) Seebeck coefficient S and (c), (d) power factor σS^2 of Ga_2TiCl_6, Ga_2TiBr_6, and Ga_2TiI_6 are computed versus μ (eV) and T (k).

matter scattering, heat causes a loss of energy. The subtracted values (0.15, 0.21, 0.13) of L (ω) have been described in figure 6(b), which is minimum in the visible region.

3.3. Thermoelectric properties

The vacancy-ordered double perovskites are outstanding for thermoelectric devices because of the significant Seebeck coefficient and ultralow values of lattice thermal conductivity [51, 52]. We have used the BoltzTraP code to obtain the thermoelectric parameters. The computed results versus temperature T (K) and chemical potential μ (eV) are plotted in figures 7–9. The chemical potential is the energy to move the carriers against coulomb forces. The peaks of large intensity are present on the negative side of μ (eV) compared to the positive. Thermoelectric strength has been counted by the figure of merit (ZT) scale. The values of ZT may be a little bit overestimated because the electronic part of thermal conductivity (k_{el}) has been incorporated and lattice vibrations (k_{ph}) have been omitted due to the limitations of semi-classical transport theory [53].

The findings of σ versus μ are shown in figure 7(a) and T in figure 7(b). The σ at $-0.04/-0.032/-0.015$ eV in the p-type region is at peak intensities $8.0/4.6/3.0 \times 10^5$ $1/\omega$m for $Ga_2Ti(Cl/Br/I)_6$, respectively. For the n-type region, the peaks exist at 0.2/0.17/0.12 eV with peak intensities $3.8/1.8.3.0 \times 10^5$ $1/\omega$m. The peaks in core sides (away from Fermi level) are not considered for discussion. The above debate shows that the p-type carriers are higher in concentration than the n-type region. Furthermore, it is noted that the σ increases from $0.02/0.15/0.16 \times 10^5$ $1/\omega$m at 100 K to $0.27/0.68/0.74 \times 10^5$ $1/\omega$m at 400 K for $Ga_2Ti(Cl/Br/I)_6$, respectively. Figure 7(b) shows that in the exchange of Cl by Br/I, the σ transferred to higher values because of increasing free carriers.

The trend of κ_e is analogous to σ, as illustrated in figure 7(c) for μ and in figure 7(d) for T. The κ_e is extremely low as compared to σ against both chemical shift and temperature. Therefore, κ_e/σ is found to be $10^{-6,}$ which makes them promise for thermoelectric applications.

The S is the potential raised between contact of metals due to temperature difference. Its values are drawn in figures 8(a), (b). The S has positive peaks at 0.05 eV for $Ga_2Ti(Cl/Br)_6$ and at 0.03 eV for Ga_2TiI_6. The negative peaks are at 0.13/0.08/0.04 eV for $Ga_2Ti(Cl/Br/I)_{6,}$ showing that S shifted to lower values by replacing anions. The plotting of S versus T shows 0.254/0.235/0.207 mV K^{-1} decreases to 0.240/0.187/0.195 mV K^{-1} by increasing the T, 100 K to 400 K. Furthermore, the replacement of Cl with Br/I decreases S because of increasing σ.

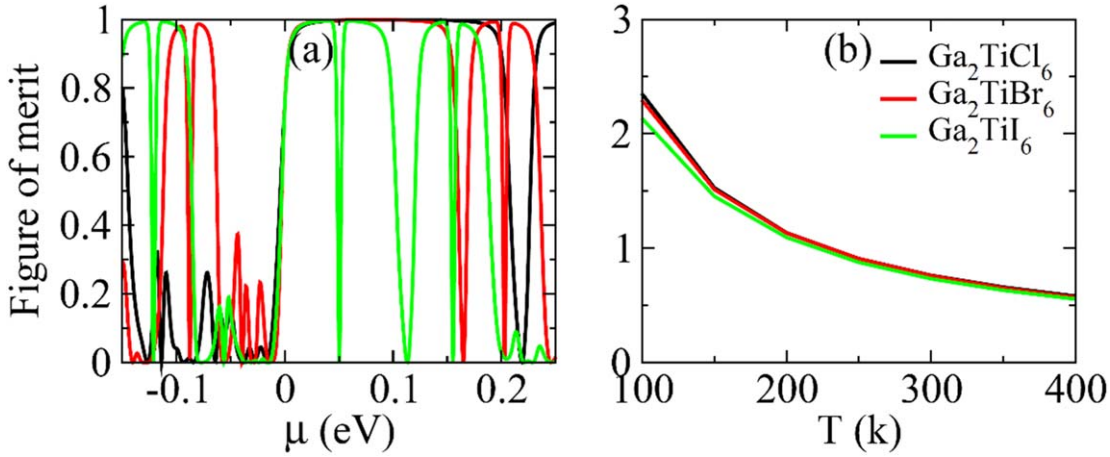

Figure 9. (a), (b) Figure of merit of Ga_2TiCl_6, Ga_2TiBr_6, and Ga_2TiI_6 is computed versus μ (eV) and T (k). The ZT has been depicted in figure 9 illustrates thermoelectric efficiency versus μ and T.

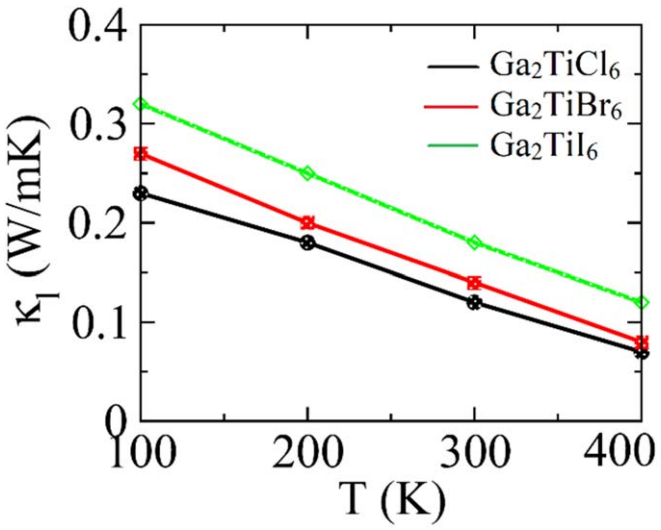

Figure 10. Lattice thermal conductivity κ_l of Ga_2TiX_6 (X = Cl/Br/I).

The strength of thermoelectric power can be understood by σS^2 (See figures 8(c), (d)). The p-type region has reached values of Power factor (PF) values from 0 to −0.11 eV, while in the n-type region, the electrons doping is less than holes. The doping values shifted to lower potential as 9.21/0.15/0.11 eV for $Ga_2Ti(Cl/Br/I)_6$. Therefore, the hole contribution is significant as compared to electrons. The PF increases with increasing T, but it follows the trends of σ because its values increase by substituting Cl with Br/I.

The ZT reaches unity in both p-type and n-type regions at different doping levels. Its values exist at large potentials for Ga_2TiCl_6 and reach to lower potential by the replacement of Cl with Br/I. The ZT versus T has been plotted in figure 9(b), which shows its values decrease by raising T. The high values at a low temperature ensure their importance for transport properties. However, to judge the effect of lattice thermal conductivity, its computed values are plotted in figure 10. The values of κ_{ph} are minimal and comparable to thermoelectric players [54, 55]. Therefore, κ_{ph} does not largely affect thermoelectric performance. The values of κ_l reported in the literature for K_2GeI_6 (0.11 W mK^{-1}), Rb_2GeI_6 (0.13 W mK^{-1}), and Cs_2GeI_6 (0.17 W mK^{-1}) [56] show the consistency with our computed values 0.11/0.13/0.17 W mK^{-1} for Ga_2TiX_6 (X = Cl, Br, I). Since, external pressure and doping both tune electronic properteis, as successfully carried out in cubic systems [57–59], such techniques are viable to pratice in the stueid materials to further mold them according to technological requirements.

4. Conclusion

Double perovskites Ga_2TiX_6 (X = Cl/Br/I) are comprehensively explored computationally for renewable solar cells and thermoelectric devices. The positive phonon frequencies show the dynamical stability, and the tolerance factor shows structural stability. The band gaps (2.74 eV, 2.0 eV, and 1.32 eV) are computed by TB-mBJ potential. The 1.32 eV for Ga_2TiI_6 is considered novel, with an absorption band of 413 nm to 689 nm in the visible region. The behavior of the real dielectric constant and refractive index is similar. Furthermore, the optical band gap and zero frequency dielectric constant are according to Penn's model. The ultralow values of thermal conductivity as compared to electrical conductivity and large figure of merit boost them for thermoelectrics. Therefore, this computational study will guide experimentalists in optimizing the performance of clean energy systems.

Acknowledgments

The authors would like to thank Taif University Researchers Supporting Project number (TURSP-2020/200), Taif University, Taif, Saudi Arabia, for supporting this project. This research was funded by the Princess Nourah bint Abdulrahman University Researchers Supporting Project number (PNURSP2022R29), Princess Nourah bint Abdulrahman University, Riyadh, Saudi Arabia. This work was also supported by King Khalid University through a grant (KKU/RCAMS/22) under the Research Center for Advanced Materials Science (RCAMS) at King Khalid University, Saudi Arabia.

Data availability statement

All data that support the findings of this study are included within the article (and any supplementary files).

ORCID iDs

Syed Awais Rouf https://orcid.org/0000-0002-8508-2572
Q Mahmood https://orcid.org/0000-0001-7449-5876

References

[1] Pareja-Rivera C, Morett D, Barreiro-Arguelles D, Olalde-Velasco P and Solis-Ibarra D 2021 Lead-free halide perovskites, beyond solar cells and LEDs *J. Phys.: Energy* **3** 032014
[2] Lei H, Hardy D and Gao F 2021 Lead-free double perovskite $Cs_2AgBiBr_6$: fundamentals *Applications, and Perspectives* **31** 2105898
[3] Pak Y, Mitra S, Almalawi D, Alwadai N, Zhang Y and Roqan I S 2019 Self-patterned $CsPbBr_3$ nanocrystals for high-performance optoelectronics B Xin *ACS Appl. Mater. Interfaces* **11** 5223–31
[4] Ajia I A *et al* AlGaN multiple quantum wells grown on transparent and conductive (−201)-oriented β-Ga_2O_3 substrate for UV vertical light emitting devices *Appl. Phys. Lett.* **113** 2018082102
[5] Ajia I A, Edwards P R, Pak Y, Belekov E, Roldan M A, Wei N, Liu Z, Robert W, Martin I S and Roqan 2017 Generated carrier dynamics in V-pit-enhanced InGaN/GaN light-emitting diode *ACS Photonics* **5** 820–6
[6] Le A T, Dinh T B, Do T A T, Ho T G, Le D M and Man M T 2022 Lattice dynamics of double perovskite Cs_2SnCl_6 from first principles and experimental studies *Mater. Lett.* **309** 131386
[7] Kojima A, Teshima K, Shirai Y and Miyasaka T 2009 Organometal halide perovskites as visible-light sensitizers for photovoltaic cells *J. Am. Chem. Soc.* **131** 6050–1
[8] Kim H S *et al* 2012 Lead iodide perovskite sensitized all-solid-state submicron thin film mesoscopic solar cell with efficiency exceeding 9% *Sci Rep.* **2** 6022–5
[9] Jeon N J, Noh J H, Yang W S, Kim Y C, Ryu S, Seo J and Seok S I 2015 Compositional engineering of perovskite materials for high-performance solar cells *Nature* **517** 476–80
[10] Luo D *et al* 2018 Enhanced photovoltage for inverted planar heterojunction perovskite solar cells *Science* **360** 1442
[11] Yoo J J, Seo G and Chua M R 2021 Efficient perovskite solar cells via improved carrier management *Nature* **590** 587–93
[12] Yang Y and You J 2017 Make perovskite solar cells stable *Nature* **544** 155
[13] Hebig J C, Kuhn I, Flohre J and Kirchartz T 2016 Optoelectronic properties of $(CH_3NH_3)_3Sb_2I_9$ thin films for photovoltaic applications *ACS Energy Lett.* **1** 309–14
[14] Singh T, Kulkarni A, Ikegami M and Miyasaka T 2016 Effect of electron transporting layer on bismuth-based lead-free perovskite $(CH_3NH_3)_3Bi_2I_9$ for photovoltaic applications *ACS Appl. Mater. Interfaces* **8** 14542–7
[15] You J *et al* 2016 Improved air stability of perovskite solar cells via solution processed metal oxide transport layers *Nat. Nanotech.* **11** 75–81
[16] Saliba M *et al* 2016 Incorporation of rubidium cations into perovskite solar cells improves photovoltaic performance *Science* **354** 5557
[17] Flora G, Gupta D and Tiwari A 2012 Toxicity of lead: a review with recent updates *Interdiscip. Toxicol.* **5** 47–58
[18] Flemban T H, Zelai T, Mahmood Q, Aravindh Sasikala Devi A, Sajjad M, Alhossainy M H, Somaily H H, Mera A, Alharthi S and Amin Mohammed A 2022 Half-metallic ferromagnetism and thermoelectric properties of double perovskites $Rb_2Z(Cl/Br)_6$ (Z = Ta, W, Re) *J. Alloys Compd.* **894** 162313

[19] Ghrib T, Rached A, Algrafy E, Al-nauim I A, Albalawi H, Ashiq M G B, Ul Haq B and Mahmood Q 2021 A new lead-free double perovskites $K_2Ti(Cl/Br)_6$; a promising materials for optoelectronic and transport properties; probed by DFT *Mater. Chem. Phys.* **264** 124435
[20] Krishnamoorthy T *et al* 2015 Lead-free germanium iodide perovskite materials for photovoltaic applications *J. Mater. Chem. A* **3** 23829–32
[21] Faizan M, Bhamu K C, Murtaza G, He X, Kulhari N, AL-Anazy M M and Khan S H 2021 Electronic and optical properties of vacancy ordered double perovskites A_2BX_6 (A = Rb, Cs; B = Sn, Pd, Pt; and X = Cl, Br, I): a first principles study *Sci. Rep.* **11** 1–9
[22] Zhou J *et al* Lead-free perovskite derivative $Cs_2SnCl_{6-x}Br_x$ single crystals for narrowband photodetectors *Adv. Optical Mater.* **1** 20191900139
[23] Cai Y *et al* 2017 Computational study of halide perovskite-derived A2BX6 inorganic compounds: chemical trends in electronic structure and structural stability *Chem. Mater.* **29** 7740–9
[24] Maughan A E, Ganose A M, Almaker M A, Scanlon D O and Neilson J R 2018 Tolerance factor and cooperative tilting effects in vacancy-ordered double perovskite halides *Chem. Mater.* **30** 3909–19
[25] Kaltzoglou A, Perganti D, Antoniadou M, Kontos A G and Falaras P 2016 Stress tests on dye-sensitized solar cells with the Cs_2SnI_6 defect perovskite as hole-transporting material *Energy Procedia* **102** 49–55
[26] Deng J, Li J, Yang Z and Wang M 2019 All-inorganic lead halide perovskites: a promising choice for photovoltaics and detectors *J. Mater. Chem. C* **7** 12415–40
[27] Wang Y, Tu J, Li T, Tao C, Deng X and Li Z 2019 Convenient preparation of $CsSnI_3$ quantum dots, excellent stability, and the highest performance of lead-free inorganic perovskite solar cells so far *J. Mater. Chem. A* **7** 7683–90
[28] Zhao X, Tang Y L, Tang T Y, Diao X F, Gao L K, Xie Q, Shi B, Yuan L and Lu L M 2021 Study on mechanical, electronic and optical properties of Pb-free double halide perovskites In_2TiX_6 (X = Cl, Br, I) for solar cells based on first-principles, Materials Today *Communications* **26** 102180
[29] Wang X D *et al* 2019 *In situ* construction of a Cs2SnI6 perovskite nanocrystal/SnS2 nanosheet heterojunction with boosted interfacial charge transfer. *J. Am. Chem. Soc.* **141** 13434–41
[30] Blaha P, Schwarz K, Sorantin P and Trickey S K 1990 Full potential, linearized augmented plane wave programs for crystalline systems *Comput. Phys. Commun.* **59** 339
[31] Tran F and Blaha P 2009 Accurate band gaps of semiconductors and insulators with a semilocal exchange-correlation potential *Phys. Rev. Lett.* **102** 22640
[32] Heyd J, Scuseria G E and Ernzerhof M 2003 Hybrid functionals based on a screened coulomb potential *J. Chem. Phys.* **118** 8207
[33] Madsen G K H, Schwarz K and Singh D J 2006 Boltz TraP a code for calculating band-structure dependent quantities *Comput. Phys. Commun.* **175** 67
[34] Jain A, Ong S P, Hautier G, Chen W, Richards W D, Dacek S, Cholia S, Gunter D, Skinner D, Ceder G and K A Persson (equal contributions) 2013 The materials project: a materials genome approach to accelerating materials innovation *APL Mater.* **1** 011002
[35] Greenwood N N and Earnshaw A 1984 *Chemistry of the Elements* Second Edition (UK: University of Leads) p 240
[36] Lai C F, Chang Y C and Tien Y C 2021 Stable lead-free cesium tin halide double-perovskite nanocrystals embedded in polydimethylsiloxane for candlelight light-emitting diodes *ACS Appl. Nano Mater.* **4** 1924–31
[37] Young J and Rondinelli J 2016 Octahedral rotation preferences in perovskite iodides and bromides *Phys. Chem. Lett.* **7** 918–22
[38] Mustafa G M, Noor N A, Iqbal M W, Sajjad M, Naeem M A, Mahmood Q, Shaikh H M, Mahmood A and Al-Masry W 2020 *Mat. Sci. Sem. Process.* **121** 105452
[39] Abbas S A, Mahmood I, Sajjad M, Noor N A, Mahmood Q, Naeem M A, Mahmood A and Ramay S M 2020 *Chem. Phys.* **538** 1109022
[40] Mahmood Q, Nazir G, Bouzgarroud S, Aljameel A I, Rehman A, Albalawi H, Haq B U, Ghrib T and Mera A 2022 Study of new lead-free double perovskites halides Tl_2TiX_6 (X = Cl, Br, I) for solar cells and renewable energy devices *J. Solid State Chemistry* **308** 122887
[41] Jong U G, Yu C J and Kye Y H 2020 Computational prediction of structural, electronic, and optical properties and phase stability of double perovskites K_2SnX_6 (X = I, Br, Cl) *RSC Adv.* **10** 201
[42] Jong U G, Yu C J, Kye Y H, Choe S H, Kim J S and Choe Y G 2019 Anharmonic phonons and phase transitions in the vacancy-ordered double perovskite Cs_2SnI_6 from first-principles predictions *Phys. Rev. B* **99** 184105
[43] Muhammed M M, Alwadai N, Lopatin S, Kuramata A and Roqan I S 2017 High-efficiency InGaN/GaN quantum well-based vertical light-emitting diodes fabricated on β-Ga_2O_3 substrate *ACS Appl. Mater. Interfaces* **9** 34057–63
[44] Alfaraj N, Mitra S, Wu F, Ajia I A, Janjua B, Prabaswara A, Aljefri R A and Sun H Photoinduced entropy of InGaN/GaN pin double-heterostructure nanowires *Appl. Phys. Lett.* **110** 161110
[45] Mahmood Q, Ghrib T, Rached A, Laref A and Kamran M A 2020 A new lead-free double perovskites $K_2Ti(Cl/Br)_6$; a promising material for optoelectronic and transport properties; probed by DFT *Mater. Sci. Semicond. Process.* **112** 105009
[46] Fox A M 2001 *Optical Properties of Solids* (UK: Oxford University Press)
[47] Wooten F 1972 *Optical Properties of Solids* (New York: Academic)
[48] Penn D R 1962 Wave-number-dependent dielectric function of semiconductors *Phys. Rev.* **128** 2093
[49] Kozak M I, Zhikharev V N, Puga P P and Loya V Y 2017 The kramers-kronig relations: validation via calculation technique *Int. J. Inno. Sci. Eng. Techn* **4** 152–9
[50] Hilal M, Khan S H and Khan A 2016 Investigation of electro-optical properties of InSb under the influence of spin–orbit interaction at room temperature *Mater. Chem. Phys.* **184** 41–8
[51] Singh D, Sajjad M, Larsson J A and Ahuja R 2020 *Results in Physics* **19** 103584
[52] Shafique A, Sharma S, Sajjad M and Schwingenschlögl, U 2021 Multivalley band structure and phonon-glass behavior of TlAgTe *ACS Appl. Energy Mater.* **4** 2174
[53] Reshak H and Auluck S 2015 Thermoelectric properties of nowotny-Juza NaZnX (X = P, As and Sb) compounds *Compute. Mater. Sci.* **96** 90–5
[54] Hellman O and Broido D A 2014 Phonon thermal transport in Bi_2Te_3 from first principles *Phys. Rev. B* **90** 134309
[55] Tian Z, Garg J, Esfarjani K, Shiga T, Shiomi J and Chen G 2012 Phonon conduction in PbSe, PbTe, and $PbTe_{1-x}Se_x$ from first-principles calculations *Phys. Rev. B* **85** 184303
[56] Al-Muhimeed T I, Shafique A, AlObaid A A, Morsi M, Nazir G, AL-Anazy M M and Mahmood Q 2021 New lead-free double perovskites X_2GeI_6 (X = K, Rb, Cs) for solar cells, and renewable energy as an alternate of hybrid perovskites *Int. J. Energ. Research* **45** 19645–52
[57] Nazir S, Mahmood I, Noor N A, Laref A and Sajjad M 2019 *High Energy Density Phys.* **33** 100715
[58] Sajjad M, Alay-e-Abbas S M, Zhang H X, Noor N A, Saeed Y, Shakir Imran and Shaukat A 2015 *J. Mag. Mag. Mater.* **390** 78
[59] Mahmood Q, Hassan M, Murtaza G, Sajjad M, Laref A and Haq B 2019 *Superconductivity and Novel Magnetism* **32** 1231–9